ARTICLE

Novel Counter Electrode V_2O_5/Al for Solid Dye-Sensitized Solar Cells

Jiangbin Xia,*,† Chaochen Yuan,† and Shozo Yanagida*,‡

College of Chemistry and Molecular Science, Wuhan University, Wuhan 430072, China, and Center for Advanced Science and Innovation, Osaka University, Suita, Osaka 565-0871, Japan

ABSTRACT High work function material V_2O_5 with Al as a composite electrode is applied first as counter electrode in solid dye-sensitized solar cell (solid DSC). Such novel counter electrode gives over 2% conversion efficiency, which is comparable with noble Ag counter electrode. In addition, such novel electrode and concept would be widely used as counter electrode in other noniodine-based solid DSCs. The replacement of regular Au, Ag noble metal electrodes gives a way to reduce the cost of solid DSC in large scale production.

KEYWORDS: dye-sensitized • counter electrode • solid state • vanadium(V) oxide

1. INTRODUCTION

Along with the upcoming industrialization of dye-sensitized solar cell, it is necessary to develop more cost-effective materials. Although most research groups or companies have already produced up to 10% of conversion efficiency in small-sized devices, solvent evaporation and iodine sublimation are the biggest obstacles in liquid DSC for practical application. Therefore, solid DSC (1−9) becomes a hot topic in this area because of its advantages of avoiding leakage or sealing problems existing in traditional liquid-based solar cells. Intensive study in this domain in academia is as important as in industry. In 1998, Grätzel et al. demonstrated this solid DSC device by using a doped small molecule hole transport layer (HTL) like 2,2′,7,7′-tetrakis(*N*,*N*-di-*p*-methoxyphenyl-amine)9,9′-spirobifluorene (Spiro-OMeTAD) (3). Meanwhile, conductive polymer such as polypyrrole (4) and poly(3,4-ethylenedioxythiophene) (PEDOT) were developed in solid DSC with great progress (6).

Generally, in these solid DSCs, noble metal electrodes such as Au and Ag (10) are as important as Pt catalyst in liquid DSC. However, a few studies were carried out to replace these expensive metal electrodes in solid DSC (2, 11). Therefore, intense investigation should be done to develop novel counter electrodes for solid DSC and new concept or design strategy are needed in this field as well. It is noted that most counter electrodes developed so far in solid DSC have high work function values, which means that high work function material may play an important role in these devices for hole extraction. In this paper, we present the application of V_2O_5/Al as novel counter electrodes with an economic way in solid DSC.

* Corresponding author. E-mail: jbxia@whu.edu.cn (J.X.); yanagida@mls.eng.osaka-u.ac.jp (S.Y.).
Received for review April 29, 2010 and accepted June 24, 2010
† Wuhan University.
‡ Osaka University.
DOI: 10.1021/am100380w

2. EXPERIMENTAL SECTION

Before coating mesoporous TiO_2 layer, a compact TiO_2 layer was deposited following the procedure described in literature (5). Mesoscopic TiO_2 electrodes were prepared on FTO (Dyesol, SnO_2: F, 8 ohm/sq) from the colloidal Nanoxide-T paste (Solaronix) by doctor-blade techniques. The films were annealed at 450 °C for 30 min in air followed by the 0.04 M $TiCl_4$ treatment. The resulting TiO_2 films (thickness is around 2.5 μm, measured by a XP-1 profiler, Ambios, Tech) were cut into pieces. The electrodes were then immersed into 3.0×10^{-4} M *cis*-bis(isothiocyanato)(2,2-bipyridyl-4,4-dicarboxylato)(2,2-bipyridyl-4,4-dinonyl)ruthenium(II) (known as Z-907, Solaronix) in acetonitrile/*tert*-butanol (1:1) for 18 h. The hole conductor layer was prepared by spin-coating a solution of Spiro-OMeTAD (0.17 M) in chlorobenzene, containing 4-*tert*-butylpyridine (0.13 M), and $Li(CF_3SO_2)_2N$ (0.021 M) (12). Generally, we spun-coat Spiro-OMeTAD solution at 2000 rpm. Finally, a 100 nm thick Ag electrode was evaporated on top of the hole conductor as a reference device (active area is 0.09 cm^2). In the case of novel counter electrodes, 5−20 nm V_2O_5 was vapor deposited on the top of Spiro-OMeTAD layer followed by 100 nm of Al deposited as back contact. Atomic force microscopy was performed using a Dimension 3100 (Nanoscope, Digital Instruments, Santa Barbara, CA) with tapping mode. The electrical impedance spectra (EIS) of all solid DSC cells were measured with an impedance analyzer (Princeton Applied Research, 1025) connected with a potentiostat (Princeton Applied Research, 273A) under dark conditions at 25 °C. The EIS was recorded over a frequency range of 0.1 to 1×10^6 Hz. The ac amplitude and the applied voltage were set to 10 and −700 mV for the cells, respectively. The performance of the DSCs were studied by recording the current−voltage (*I*−*V*) characteristics of the unsealed type cell under illumination of AM1.5 (1 Sun; 100 mW/cm^2) using a solar simulator (Newport, 91160). The data were obtained from the average of at least three examples.

3. RESULTS AND DISCUSSION

3.1. AFM Image and Energy Level Diagram.

Typical AFM images of spin-coated Spiro-OMeTAD and V_2O_5 covered Spiro-OMeTAD are shown in Figure 1. Images b and d in Figure 1 are the magnification for images

Published on Web 07/08/2010

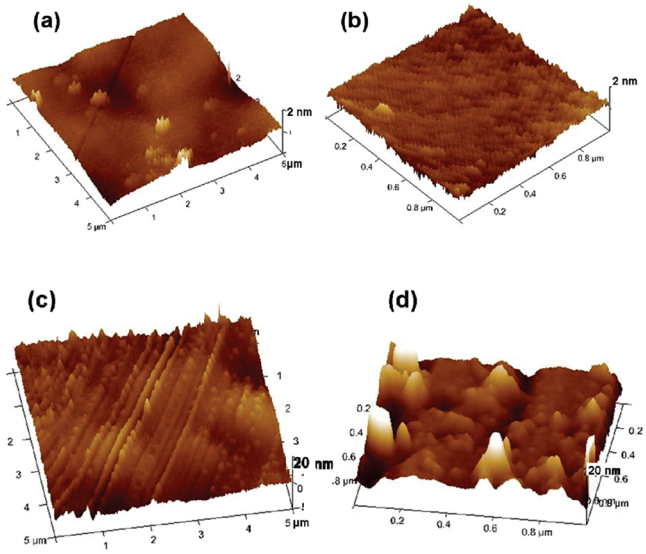

FIGURE 1. AFM image of (a, b) spin-coated Spiro-OMeTAD layer and (c, d) 10 nm V_2O_5 deposited on Spiro-OMeTAD at 0.5 Å/s.

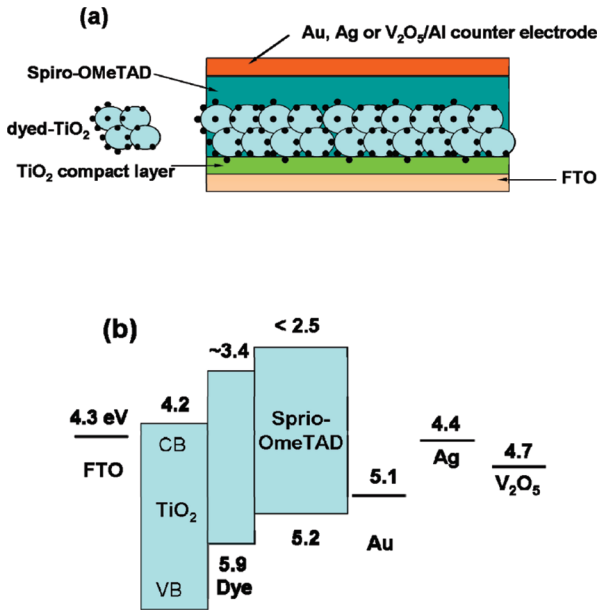

FIGURE 2. Schematic views of solid DSC devices' structure and energy level of materials.

a and c in Figure 1, respectively. Images a and b in Figure 1 show that the surface of spin-coated Spiro-OMeTAD is very flat and uniform, although some islands are found in this film. In the case of V_2O_5 covered on Spiro-OMeTAD film as shown in images c and d in Figure 1, we can observe uniform strips of V_2O_5, which is the evidence of V_2O_5 growth on Spiro-OMeTAD layer. Meanwhile, compared with Spiro-OMeTAD layer surface, V_2O_5 films show a rougher surface and 120 nm wide gap between the neighboring strips. The 15 and 20 nm V_2O_5 deposition demonstrate similar strips. Figure 2 shows the schematic views of a typical solid DSC device structure and its band level diagram.

3.2. Photovoltaic Performance with Different Counter Electrodes. The $I-V$ curves obtained from different V_2O_5 thickness combing with Al as well as Ag-

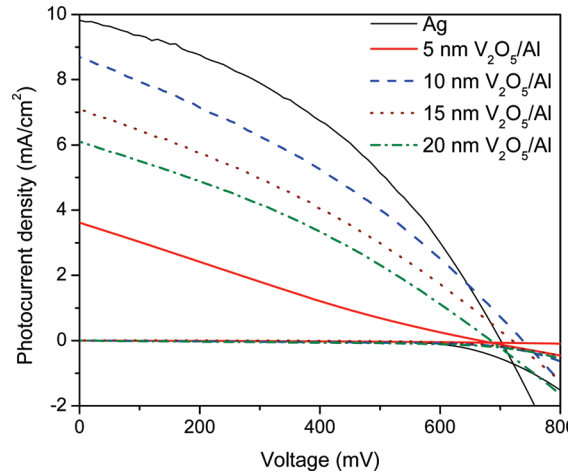

FIGURE 3. $I-V$ curves of solid-DSC based on different counter electrodes.

Table 1. Summary of the Photovoltaic Properties of the Solid DSCs

counter electrode	J_{sc}(mA/cm^2)	V_{oc} (mV)	FF	η %
Ag	9.6 ± 0.4	710 ± 10	0.39 ± 0.02	2.6 ± 0.1
Al				0
5 nm V_2O_5/Al	3.8 ± 0.5	670 ± 10	0.22 ± 0.03	0.58 ± 0.1
10 nm V_2O_5/Al	8.0 ± 0.5	730 ± 10	0.34 ± 0.02	2.0 ± 0.1
15 nm V_2O_5/Al	7.1 ± 0.3	713 ± 15	0.32 ± 0.02	1.63 ± 0.1
20 nm V_2O_5/Al	5.9 ± 0.3	690 ± 15	0.34 ± 0.04	1.39 ± 0.2

based solid DSC are shown in Figure 3, and their parameters are listed in Table 1. When pure Al works as the counter electrode, most devices are short-circuited. It is acceptable that the internal electrical field under irradiation is the driving force for holes and electrons moving toward the anode and cathode electrode in polymer solar cell. Generally, the internal electrical field is primary determined by the workfunction difference between the anode and cathode materials when the active layers thickness are the same. Here in Al alone as counter electrode device, the work function difference between FTO (4.3 eV) and Al (4.3 eV) is around zero, which leads to short-circuiting of the device. Taking unidirectional electron flow in the devices into consideration, we would be better to use high work function material to extract hole when Spiro-OMeTAD employed as p-type hole conductor in solid DSC. Therefore, low work function Al alone is a bad choice for solid Spiro-OMeTAD-based DSC counter electrode.

It is clear that the $I-V$ properties of the devices are sensitive to V_2O_5 thickness. Generally, all devices based on these novel counter electrodes shows poorer FF compared with Ag counter electrode. When 5 nm of V_2O_5 was deposited on Spiro-OMeTAD, we can get 0.6% of efficiency with poorer J_{sc} which is lower than 5.0 mA/cm^2. However, 10 nm thick V_2O_5 gives a V_{oc} of 730 mV and J_{sc} of 8.0 mA/cm^2; accordingly, the best performance is up to 2% of efficiency, which is around 80% of efficiency based on noble Ag counter electrode. This result is promising that we have developed a novel counter elec-

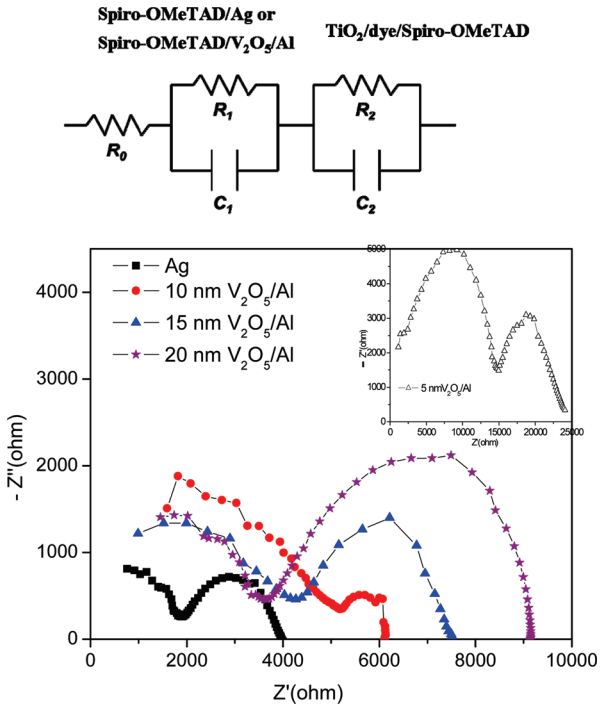

FIGURE 4. Electrochemical impedance spectra of solid DSC with different counter electrode: Ag (square), 5 nm V_2O_5/Al (open triangle), 10 nm V_2O_5/Al (circle), 15 nm V_2O_5/Al (solid triangle), and 20 nm V_2O_5/Al (star). The equivalent circuit is shown on the top of the figure.

trode for solid DSC. Along with the further increase in V_2O_5 thickness, the device gives poorer performance especially in J_{sc} and V_{oc}. We attribute this to the resistivity of thicker V_2O_5 layer. Although the high work function interface layer that is reactive to both Al and Spiro-OMeTAD plays a key role in such a novel counter electrode, we need to deposit appropriate thickness of V_2O_5. If the V_2O_5 layer is too thin to fully cover Spiro-OMeTAD layer, it would result in short-circuiting by the subsequently deposited Al. Interestingly, it seems that the devices employed by V_2O_5/Al counter electrode show higher V_{oc} with 20−30 mV of improvement. This can be well-explained by the higher work function value of V_2O_5 (4.7 eV) compared with that of Ag (4.4 eV) or formation of surface dipoles between V_2O_5 and Spiro-OMeTAD layer.

As we discussed before (13), solid DSC is very similar to polymer thin film solar cell. For instance, hole−electron separation occurs at the interface between PCBM and P3HT in polymeric solar cell, whereas in solid DSC, dyed TiO_2 serves as the light harvester and electron transporting layer, and then charge separation takes place at the interface between dyed TiO_2 and hole conductors. Compared with polymer solar cell, the dye molecules play a decisive role in light harvest. Therefore, anode electrodes employed in organic thin film solar cells (polymer solar cells) will be useful especially in solid DSC when hole conducting materials like Spiro-OMeTAD and P3HT are introduced as a substitute for iodide/iodine electrolytes. Fortunately, Hou et al. (14) developed C60/Al composite anode, whereas Yang et al. (15, 16) demonstrated V_2O_5/Al in inverted organic solar cell. Although we have tried C60/Al as a counter electrode in Spiro-OMeTAD based solid DSC and have got similar results, V_2O_5 is more stable in air and much cheaper than C60. Here, our experiments demonstrate that high work function material combined with Al would be an excellent economic counter electrode in solid DSC. It is reasonable that interface-active and high work function V_2O_5 layer materials with work function of 4.7 eV can collect hole efficiently as well as Au (5.1 eV), carbon (4.4−5.2 eV), and C60/Al (5.2 eV) (14) when solid DSC devices are in working conditions. Compared with liquid iodide/iodine-based DSC, the interface contact between solid Spiro-OMeTAD electrolyte and counter electrode (like Au and Ag as well as V_2O_5/Al) and band level matching (shown in Figure 2b) are more important for device operation.

3.3. Impedance of the Solid DSCs. As shown in Figure 4, two semicircles were observed in the measured frequency range of 1×10^{-1} to 1×10^{5} Hz for all devices. Five nm V_2O_5/Al is shown as inset in the Figure. The results are based on the equivalent circuits shown at the top of Figure 4. The equivalent circuits of DSCs can be represented by two RC circuits in parallel, in good agreement with previously published work (17). The observed R and C values obtained after fitting are presented in Table 2.

According to the previous works (6, 17), the semicircles in the frequency regions 1×10^{3} to 1×10^{5} and 1 to 1×10^{3} Hz correspond to charge-transfer processes occurring at the counter electrode/Spiro-OMeTAD and the TiO_2/dye/Spiro-OMeTAD interface. It is obvious that Ag counter electrode shows the lowest value at the first semicircle, whereas all V_2O_5/Al systems give higher values. It is noted that 5 nm V_2O_5/Al shows the highest impedance value, which is up to 20 000 ohm; that is, in this device, R_1 and R_2 show up to 12 012 and 8329 Ω cm^2, respectively, compared with other systems. We attribute this result to the nonhomogeneous coverage of V_2O_5 and the penetration of low work function material Al into V_2O_5 or Spiro-OMeTAD hole conductor. Combining with the fact that 5 nm V_2O_5/Al also

Table 2. Parameters Obtained by Fitting the Impedance Spectra of Different Solid DSCs Shown in Figure 4 Using the Equivalent Circuit

	R_0 (Ω cm^2)	R_1 (Ω cm^2)	C_1 (F cm^{-2})	R_2 (Ω cm^2)	C_2 (F cm^{-2})
Ag	470.5	1458	2.43×10^{-9}	1891	1.63×10^{-6}
5 nm V_2O_5/Al	1801	12012	1.37×10^{-9}	8329	8.31×10^{-7}
10 nm V_2O_5/Al	986.8	3673	1.14×10^{-9}	1365	1.07×10^{-6}
15 nm V_2O_5/Al	1189	2897	2.44×10^{-9}	3119	1.56×10^{-6}
20 nm V_2O_5/Al	1018	2750	1.37×10^{-9}	5092	8.12×10^{-7}

exhibits the poorest performance in solid DSC (shown in Figure 3 and Table 1), we can imagine that a small amount of Al would penetrate into thinner V_2O_5 and Spiro-OMeTAD layer, which will result in short circuit and poor hole extraction to the external circuit. Along with the further increase V_2O_5 thickness, the diameter of the first circle decreases and fitted R_1 value gradually declines to 3673 Ω cm^2 and finally stabilizes around 2800 Ω cm^2. Interestingly, in the case of 10 nm V_2O_5/Al system, it gives a much smaller second circle even compared with the Ag counter electrode system as reflected in Table 2. This might be due to V_2O_5 playing a helpful role in the hole extraction in the devices. That is, V_2O_5 would be beneficial to the charge transfer to TiO_2/dye/Spiro-OMeTAD/10 nmV_2O_5 interface. Taking the consideration of poorer conductivity of V_2O_5 layer, its device performance is a little bit lower than that based on Ag counter electrode. Finally, in the case of 20 nm V_2O_5/Al system, V_2O_5 forms a new phase with fully coverage on Spiro-OMeTAD layer. Therefore, it has almost no further effect on charge transfer of the counter electrode/Spiro-OMeTAD, as reflected in the first circle in Figure 4 and fitted value in Table 2. Meanwhile, the newly formed V_2O_5 phase will increase the resistivity of the devices with large enhancement of impedance value, as shown in the second circle in the impedance spectra (in the case of 15 and 20 nm of V_2O_5).

Taking the AFM picture into consideration in Figure 1, 10 nm of V_2O_5 tends to form strips, which means that V_2O_5 forms nonhomogeneous coverage on the Spiro-OMeTAD film because of the phase separation between the organic Spiro-OMeTAD phase and the V_2O_5 phase. Therefore, higher efficiency will be expected once the surface is further modified or the codoping method is applied to tune the interface between the Spiro-OMeTAD and V_2O_5 phase.

CONCLUSIONS

In summary, we have demonstrated that V_2O_5/Al can be successfully used as a novel counter electrode in Spiro-OMeTAD-based solid DSC. We can replace Ag noble counter electrode by V_2O_5/Al and it is an economic choice, as the latter costs only one-tenth that of Ag or even less. Furthermore, such novel electrode and concept would be widely used as counter electrode in other noniodine-based solid DSCs. Once again, the interface engineering is a powerful means to let hole extraction occur unidirectionally during fabrication of the counter electrode in solid DSC.

Acknowledgment. This work was supported by the startup fund from Wuhan University, and New Energy and Industrial Technology Development Organization (NEDO) under the Ministry of Economy, Trade and Industry. The authors also thank Prof. Anvar Zakhidov for helpful discussion and technical support.

REFERENCES AND NOTES

(1) Tennakone, K.; Kumara, G. R. A.; Kottegoda, I. R. M.; Wijayantha, K. G. U.; Perera, V. P. S. *J. Phys. D: Appl. Phys.* **1998**, *31*, 1492.
(2) O'Regan, B.; Schwartz, D. T.; Zakeeruddin, S. M.; Grätzel, M. *Adv. Mater.* **2000**, *12*, 1263.
(3) Bach, U.; Lupo, D.; Comte, P.; Moser, J. E.; Weissörtel, F.; Salbeck, J.; Spreitzer, H.; Grätzel, M. *Nature* **1998**, *395*, 583.
(4) Murakoshi, K.; Kogure, R.; Wada, Y.; Yanagida, S. *Chem. Lett.* **1997**, *26*, 471.
(5) Saito, Y.; Kitamura, T.; Wada, Y.; Yanagida, S. *Synth. Met.* **2002**, *131*, 185.
(6) (a) Xia, J.; Masaki, N.; Lira-Cantu, M.; Kim, Y.; Jiang, K.; Yanagida, S. *J. Am. Chem. Soc.* **2008**, *130*, 1258. (b) Yanagida, S.; Yu, Y.; Kazuhiro, M. *Acc. Chem. Res.* **2009**, *42*, 1827.
(7) Karthikeyan, C. S.; Wietasch, H.; Thelakkat, M. *Adv. Mater.* **2007**, *19*, 1091.
(8) Tan, S. X.; Zhai, J.; Wan, M. X.; Meng, Q. B.; Li, Y. L.; Jiang, L.; Zhu, D. B. *J. Phys. Chem. B* **2004**, *108*, 18693.
(9) Wang, Y. P.; Yang, K.; Kim, S. C.; Nagarajan, R.; Samuelson, L. A.; Kumar, J. *Chem. Mater.* **2006**, *18*, 4215.
(10) Snaith, H. J.; Moule, A. J.; Klein, C.; Meerholz, K.; Friend, R. H.; Grätzel, M. *Nano Lett.* **2007**, *7*, 3372.
(11) Ikeda, N.; Miyasaka, T. *Chem. Commun.* **2006**, 1886.
(12) Chen, P.; Yum, J-H; Angelis, F. D.; Mosconi, E.; Fantacci, S.; Moon, S-J; Baker, R. H.; Ko, J.; Nazeeruddin, M. K.; Grätzel, M. *Nano Lett.* **2009**, *9*, 2487.
(13) Xia, J.; Yanagida, S. *Sol. Energy* **2010**; DOI:10.1016/J.Solener.2009.10.005.
(14) Wang, M. L.; Song, Q. L.; Wu, H. R.; Ding, B. F.; Gao, X. D.; Sun, X. Y.; Ding, X. M.; Hou, X. Y. *Org. Electron.* **2007**, *8*, 445.
(15) Li, G.; Chu, C.-W.; Shrotriya, V.; Huang, J.; Yang, Y. *Appl. Phys. Lett.* **2006**, *88*, 253503.
(16) Liao, H.-H.; Chen, L.-M.; Xu, Z.; Li, G.; Yang, Y. *Appl. Phys. Lett.* **2008**, *92*, 173303.
(17) Han, L.; Koide, N.; Chiba, Y.; Mitate, T. *Appl. Phys. Lett.* **2004**, *84*, 2433.

AM100380W